

# Remodeling of the Folding Free Energy Landscape of Staphylococcal Nuclease by Cavity-Creating Mutations

Julien Roche,<sup>†</sup> Mariano Dellarole,<sup>†</sup> Jose A. Caro,<sup>‡</sup> Ewelina Guca,<sup>†</sup> Douglas R. Norberto,<sup>§</sup> Yinshan Yang,<sup>†</sup> Angel E. Garcia,<sup>⊥</sup> Christian Roumestand,<sup>†</sup> Bertrand García-Moreno,<sup>‡</sup> and Catherine A. Royer<sup>\*,†</sup>

<sup>†</sup>Centre de Biochimie Structurale, INSERM U554, CNRS UMR 5048, Universités de Montpellier, Montpellier, France

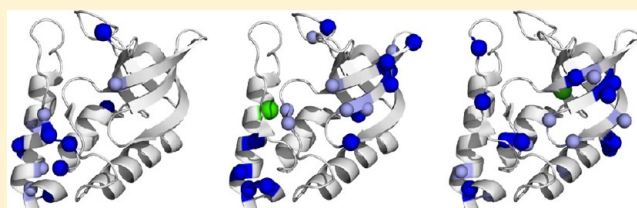
<sup>‡</sup>Department of Biophysics, Johns Hopkins University, Baltimore, Maryland 21218, United States

<sup>§</sup>Department of Biochemistry, Institute of Biology, University of Campinas, Campinas, Brazil

<sup>⊥</sup>Department of Physics and Applied Physics and Center for Biotechnology and Interdisciplinary Studies, Rensselaer Polytechnic Institute, Troy, New York 12180, United States

## **S** Supporting Information

**ABSTRACT:** The folding of staphylococcal nuclease (SNase) is known to proceed via a major intermediate in which the central OB subdomain is folded and the C-terminal helical subdomain is disordered. To identify the structural and energetic determinants of this folding free energy landscape, we have examined in detail, using high-pressure NMR, the consequences of cavity creating mutations in each of the two subdomains of an ultrastable SNase,  $\Delta$ +PHS. The stabilizing mutations of  $\Delta$ +PHS enhanced the population of the major folding intermediate. Cavity creation in two different regions of the  $\Delta$ +PHS reference protein, despite equivalent effects on global stability, had very distinct consequences on the complexity of the folding free energy landscape. The L125A substitution in the C-terminal helix of  $\Delta$ +PHS slightly suppressed the major intermediate and promoted an additional excited state involving disorder in the N-terminus, but otherwise decreased landscape heterogeneity with respect to the  $\Delta$ +PHS background protein. The I92A substitution, located in the hydrophobic OB-fold core, had a much more profound effect, resulting in a significant increase in the number of intermediate states and implicating the entire protein structure. Denaturant (GuHCl) had very subtle and specific effects on the landscape, suppressing some states and favoring others, depending upon the mutational context. These results demonstrate that disrupting interactions in a region of the protein with highly cooperative, unfrustrated folding has very profound effects on the roughness of the folding landscape, whereas the effects are less pronounced for an energetically equivalent substitution in an already frustrated region.



Staphylococcal nuclease (SNase) has long served as a model system for protein folding.<sup>1,2</sup> It is a globular protein of moderate complexity, consisting of three structural subdomains (Figure 1A). The major N-terminal subdomain (SubD1) belongs to the OB-fold family of folds,<sup>3</sup> subdomain 2 (SubD2) corresponds to the C-terminal helix, and these domains are linked by an interfacial domain between the two subdomains (IntD). An alternative, more energetically based classification of the SNase architecture resulting from pH-dependent H/D exchange experiments using a more stable double mutant H124L+P117G<sup>4</sup> describes SNase in terms of three main foldons (Figure 1B). Rapid mixing fluorescence experiments<sup>5,6</sup> have revealed a major intermediate in SNase folding consisting of an ordered OB-subdomain and a disordered C-terminal  $\alpha$ -helix. Similar structural properties for the SNase transition state ensemble were suggested by pressure-jump kinetics experiments.<sup>7</sup> In a recent study<sup>8</sup> of cavity containing variants of a highly stable form of staphylococcal nuclease (SNase) known as  $\Delta$ +PHS, a comparison of the multiple observables provided by residue specific high-pressure NMR spectroscopy revealed significant departure from two-state behavior at equilibrium for some of the variants.

The question posed here is, how do the sequence and the structure of SNase fashion its folding free energy landscape?

In proteins such as T4 lysozyme,<sup>9,10</sup> multistep unfolding reflects the hierarchy of local stabilities encoded in the protein structure; i.e., the least stable region unfolds first. Even single-domain proteins that appear to fold in a two-state manner can exhibit clear deviations from the ideal two-state behavior when analyzed with the appropriate probes.<sup>11–14</sup> It has been proposed that the unfolding of most globular proteins proceeds through the formation of a dry molten globule intermediate, consisting of compact and dehydrated states with unlocked side chains and without disruption of secondary structures.<sup>15</sup> Folding intermediates are also important for the information they may provide about functionally important excited states. In general, understanding the structural and physical properties of folding intermediates and how their stability is encoded in the protein sequence is crucial for understanding protein folding

**Received:** August 9, 2012

**Revised:** October 10, 2012

**Published:** November 1, 2012



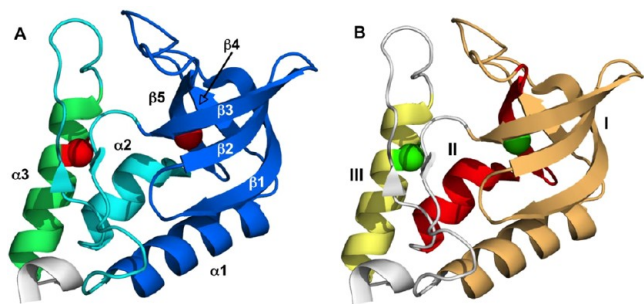


**Figure 1.** (A) Crystal structure of  $\Delta$ +PHS SNase (3BDC) with the secondary elements labeled. The subdomain organization in  $\Delta$ +PHS<sup>34</sup> is indicated as follows: SubD1 consisting of the first 96 residues that form a 5-stranded  $\beta$ -barrel ( $\beta$ 1– $\beta$ 5) and an abutting  $\alpha$ -helix ( $\alpha$ 1) (blue), IntD (cyan) ( $\alpha$  helix 2, residues 99–105, and a mini- $\beta$ -sheet, residues 39–40 and 110–111), and SubD2 ( $\alpha$  helix 3), spanning residues 122–134 (green). The location of Ile 92 and Leu 125 is indicated with red spheres. (B) Foldon organization according to foldon I (orange,  $\beta$ 1– $\beta$ 4 +  $\alpha$ 1), foldon II (red,  $\beta$ 5 +  $\alpha$ 2), and foldon III (yellow,  $\alpha$ 3). The location of Ile 92 and Leu 125 is indicated with green spheres.

and misfolding.<sup>16–18</sup> However, direct experimental detection of these states remains extremely challenging.

Some of the most useful experimental approaches for detecting and characterizing folding intermediates in detail are based on NMR spectroscopy. For example, relaxation dispersion techniques have afforded detailed structural descriptions of excited states in exchange with the native state with a probability of 1% or greater.<sup>19–21</sup> Hydrogen/deuterium (H/D) exchange experiments can bring to light excited states that are populated with less than 0.1% probability and have allowed detection of early H-bond disruption in unfolding.<sup>22–24</sup> Coupling NMR to high pressure has provided additional insight. For example, pressure-dependent H/D exchange revealed the subdomain organization of proteins such as apocytochrome b<sub>562</sub>, where different pressure sensitivities were detected for the three folding units.<sup>25</sup> Low-lying conformational substates in the folded state manifold of several globular proteins<sup>26–31</sup> have been detected by measurement of HSQC spectra at subdenaturing pressures. Indeed, pressure perturbation can reveal conformational states on the (un)folding landscape of proteins that are obscured by heating or chemical denaturation. This is because pressure effects depend upon the presence and magnitude of solvent-excluded voids heterogeneously distributed throughout the folded conformations of proteins,<sup>8</sup> in contrast to temperature or chemical denaturants, which act globally in proportion to the change in the degree of exposure of surface area upon unfolding. Finally, site-specific mutational studies have long been used to establish the relationships between sequence, structure, stability, and folding mechanisms. In particular, substitution with Ala has been used to decipher the role of side-chain packing on global protein stability<sup>32–34</sup> as well as structural properties of the transition state and folding pathways.<sup>35</sup>

In the present work we combined pressure and cavity creation mutational perturbations with NMR spectroscopy to probe the structural determinants of the folding free energy landscape of SNase. In particular, we carried out high-pressure NMR experiments as a function of denaturant concentration on the  $\Delta$ +PHS+I92A (I92A) and  $\Delta$ +PHS+L125A (L125A) cavity containing variants relative to the  $\Delta$ +PHS protein and to the true wild-type (WT) SNase. The highly stable  $\Delta$ +PHS variant bears stabilizing substitutions in the C-terminal helix (G50F, V51N,

P117G, H124L, and S128A), and a deletion of the mobile  $\Omega$  loop (residues 44–49), which is part of the active site. We note that the energetic foldon description of SNase<sup>4</sup> is likely to be similar but not exactly the same for  $\Delta$ +PHS, which is more stable than the WT SNase by  $\sim 7$  kcal/mol.<sup>36</sup>

WT SNase exhibited nearly ideal two-state pressure-induced unfolding. Nonetheless, the multiple NMR observables combined with pressure denaturation allowed the detection at equilibrium of a small population of the major unfolding intermediate of SNase exhibiting a folded central core and disorder in the C-terminal helix. A combination of pressure-dependent H/D exchange and NMR-detected high-pressure unfolding showed that the mutations used to engineer  $\Delta$ +PHS accentuate the inherent subdomain organization of SNase, significantly stabilizing this major intermediate relative to the WT.

As reported recently,<sup>36</sup> the structural, energetic, and dynamic consequences on the native state ensemble of the two alanine substitutions, I92A and L125A, in the reference  $\Delta$ +PHS protein differ markedly despite equivalent folding stabilities ( $\Delta G_f = 7.9 \pm 0.3$  and  $8.1 \pm 0.1$  kcal/mol for I92A and L125A, respectively).<sup>36</sup> While the L125A substitution, in the C-terminal helix (foldon 3 or SubD2), leads to a local structural rearrangement of the folded state in solution, the I92A substitution, in  $\beta$ 5 (foldon 2 or SubD1), mainly increases the probability of populating higher energy conformers<sup>36</sup> in the folded state basin. Here we demonstrate that these two cavity-creating substitutions have profoundly contrasted consequences on the folding free energy landscape as well. The L125A substitution retained the major intermediate and promoted the appearance of an additional excited state with disorder in the N-terminus, but otherwise decreased landscape heterogeneity with respect to the  $\Delta$ +PHS background protein. In contrast, the I92A variant exhibited significant disruption of the energetic hierarchy of states on its folding landscape and the population of a large number of intermediates involving disorder in regions across the entire structure of the protein. Nondenaturing concentrations of guanidinium hydrochloride (GuHCl) led to suppression of the major intermediate in pressure unfolding for  $\Delta$ +PHS and L125A. However, whereas in the case of  $\Delta$ +PHS denaturant led to a general stabilization of other intermediates involving the rest of the protein, the destabilization of the interactions between subdomains in L125A resulted in a GuHCl-dependent smoothing of the folding landscape. Denaturant modified the relative stabilities of the multiple intermediates in I92A but did not significantly alter the degree of complexity of the landscape. Hence, the cooperativity of folding is relatively robust to a substitution in a region of SNase already implicated in a partially folded intermediate, but an energetically equivalent substitution in a highly unfrustrated region leads to a breakdown in cooperative folding.

## ■ MATERIALS AND METHODS

**Protein Purification.** The highly stable  $\Delta$ +PHS form of SNase and the cavity-creating variants were expressed and purified as described previously.<sup>37</sup> Uniform <sup>15</sup>N labeling was obtained from overexpression of recombinant protein in *E. coli* grown in M9 medium containing <sup>15</sup>NH<sub>4</sub>Cl as the sole nitrogen source, as described for SNase previously.<sup>38</sup>

**High-Pressure Unfolding.** Uniformly <sup>15</sup>N-labeled protein samples were dissolved at 1 mM concentration in 10 mM Tris buffer at pH 7. 10% of D<sub>2</sub>O was added for the lock procedure. In all experiments, the <sup>1</sup>H carrier was centered on the water resonance and a WATERGATE sequence<sup>39,40</sup> was incorporated

to suppress solvent resonances. All NMR spectra were processed and analyzed with GIFA.<sup>41</sup> High-pressure heteronuclear 2D <sup>15</sup>N–<sup>1</sup>H HMQC spectra<sup>42</sup> were recorded at 293 K on a 600 MHz Bruker Avance III spectrometer equipped with a 5 mm Z-gradient <sup>1</sup>H–X double-resonance broadband inverse (BBI) probe. Commercial ceramic high-pressure NMR cell and an automatic pump system (Daedalus Innovations, Philadelphia, PA) were used to vary the pressure in the 1 bar–2.5 kbar range. Under equilibrium conditions, native cross-peak intensities were integrated from the corresponding HSQC spectrum, and the resulting intensity versus pressure data points were individually fitted for each resonance, assuming a two-state transition and a linear change of the folding free energy with pressure.<sup>8</sup> The Go model simulations, constrained by the equilibrium unfolding data, were performed as previously described.<sup>8</sup>

**High-Pressure H/D Exchange.** H/D exchange experiments were performed as previously described<sup>43</sup> with freshly lyophilized samples dissolved in D<sub>2</sub>O at a concentration of 1 mM. Time series of <sup>15</sup>N–<sup>1</sup>H HMQC spectra were recorded at 600 MHz with a common dead time of 15 min and a time limit of 66 h ( $\Delta$ +PHS), 86 h (I92A), and 48 h (L125A). Protection factors<sup>44</sup> were calculated from the exchange rate constants deduced from the time dependence of peak intensities fitted to a monoexponential decay model. The acid, base, and water hydrogen exchange rate constants were corrected for the pressure effects as described by Fuentes and Wand.<sup>25</sup>  $\Delta V_x$  values were estimated from the linear decrease of the free energy of exchange with pressure.

**Go Model Simulations.** Full-length structures of  $\Delta$ +PHS and the cavity variants were constructed from crystallographic reference structures 3BDC and 3OSO, respectively, and MODELER software. A C $\alpha$  model of these proteins and the corresponding Go model parameters were generated using the SMOG@ctbp Web server.<sup>45</sup> A complete thermodynamic integration of the  $\Delta$ +PHS protein using a WHAM algorithm<sup>46,47</sup> was performed to determine the folding temperature of this model. A temperature of 0.85T<sub>f</sub> was then used. The pressure dependence was introduced through the experimentally derived fractional contact maps with a simple three-step procedure:

- 1 Based on the HSQC spectra recorded at each pressure, the probability to find a residue *i* in a folded state at a pressure *p*:  $p(i)_p$  is given by the corresponding normalized resonance intensity.
- 2 The probability to form a specific native contact between residues *i* and *j* is then simply calculated as  $p(i,j)_p = p(i)_p p(j)_p$ .
- 3 A list of native contacts is established through a random number generator by individually testing each native contact (i.e., a native contact is accepted in the list if:  $\text{rand}() < p(i,j)_p$ ). For example, if the random number between 0 and 1 is 0.4 and the contact probability is 0.6, then this contact is counted in the list. If, however, the random number generated for that contact in that list is 0.8, then the contact is not counted. This procedure was repeated 100 times, generating 100 different lists of native contacts for both models. A 100 ns long C $\alpha$  Go model simulation was finally performed independently from each list of native contacts, and the resulting conformations (400 000) were collectively analyzed based on the fraction of native contact (*Q*). Free energy profiles at several pressures were therefore reconstructed from these simulations.

## RESULTS

**High-Pressure Unfolding Monitored with NMR Spectroscopy.** Pressure-induced unfolding was monitored by recording <sup>15</sup>N–<sup>1</sup>H HSQC spectra at 20 °C, at pressures ranging from 1 to 2500 bar and at various concentrations of GuHCl and at pH 5.5 or 7, respectively, for WT or  $\Delta$ +PHS SNase variants.<sup>48</sup> Intensity profiles of all resolvable amide group cross-peaks as a function of pressure for all four proteins were well-described individually by a two-state unfolding model (Figure S1), yielding residue-specific estimates of the apparent free energy differences ( $\Delta G_u$ ) and volume changes ( $\Delta V_u = -\Delta V_f$ ) between the folded and pressure-unfolded states (Figure 2A and Figure 3A,C,E).<sup>8</sup> WT SNase exhibits moderate global stability ( $\Delta G_u(\text{wt}) \sim 3.5 \pm 0.5$  kcal/mol at pH 5.5), in good agreement with previous measurements ( $4.0 \pm 0.25$  kcal/mol) made under similar conditions, excepting the presence of 100 mM KCl.<sup>49</sup> Given this moderate stability, complete unfolding was observed below 2.5 kbar in the absence of any chemical denaturant. The average magnitude of the site specific apparent  $\Delta V_f (= -\Delta V_u)$  values obtained from fits of the HSQC intensities vs pressure for WT SNase was  $65 \pm 7$  mL/mol, in good agreement with previously reported of 65 mL/mol.<sup>50</sup> The distribution of the residue-specific apparent  $\Delta V_f$  values was fairly narrow and symmetric (Figure 2A,B), consistent with a highly cooperative unfolding transition.

Contact maps at each pressure were constructed as previously described<sup>8</sup> (see also legend to Figure S2) from the product of the fractional intensities of the HSQC peaks of the two residues involved in each contact. The unfolding intermediate with a partially disrupted C-terminal helix that was identified previously for the  $\Delta$ +PHS form of SNase<sup>8</sup> was less apparent, yet still detectable in WT SNase (Figure 2C,D). We note also that the standard deviation for the distribution of the apparent  $\Delta V_f$  values for the WT ( $\sim 6.2$  mL/mol) is slightly larger than the average uncertainty in each of their values ( $\pm 4.3$  mL/mol), indicating a persistent, low level of heterogeneity.

The pressure unfolding of the  $\Delta$ +PHS variant exhibited values of  $\Delta V_f$  similar to those obtained for the WT SNase (Figure 3A,B). However, unlike that for WT SNase, and as reported previously<sup>8</sup> and presented here for comparison, the distribution of apparent  $\Delta V_f$  values for  $\Delta$ +PHS at 1.5 M GuHCl is highly asymmetric, indicative of significant deviation from two-state behavior, and enhanced population of the major unfolding intermediate with a partially disrupted C-terminus and an intact central core. Increasing GuHCl to 2 M led to a more symmetric and broad distribution of  $\Delta V_f$  values and shifted it to higher average values. As can be seen in the fractional contact maps obtained for this concentration of GuHCl at several pressures (Figure 4A–C), the contact heterogeneity becomes apparent in several other regions of the protein and is diminished for the major intermediate. As previously,<sup>8</sup> we used the fractional contacts to randomly generate contact lists and then ran Go model folding/unfolding simulations using these lists. While at low GuHCl, as previously reported, the intermediate is apparent in the free energy profile, it is nearly completely suppressed by 2 M GuHCl (Figure S2). The standard deviation for the distribution of  $\Delta V_f$  values ( $\sim 14.2$  mL/mol) at high denaturant remains larger than the average uncertainty in their measurement ( $\pm 9.8$  mL/mol).

As previously reported,<sup>8</sup> cavity-creating substitutions in the  $\Delta$ +PHS protein led to larger values for the average apparent  $\Delta V_f$  (Figure 3C–F). The L125A variant, which contains an

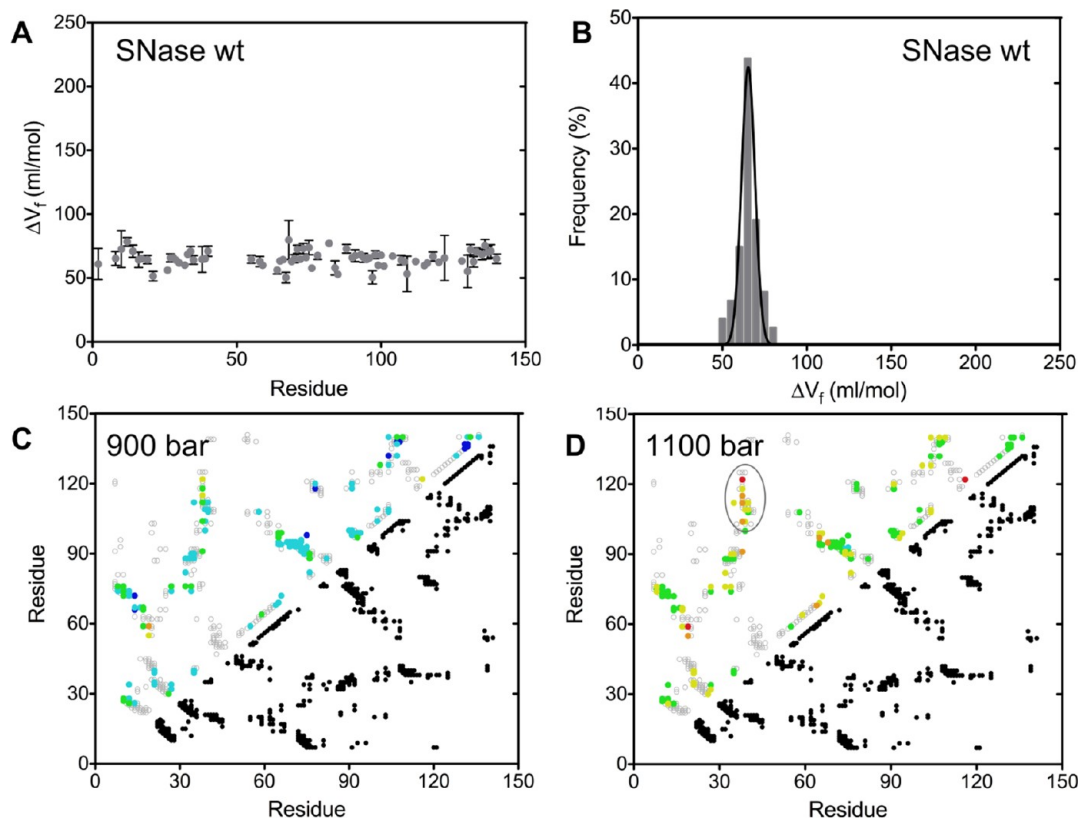


**Figure 2.** Pressure-induced unfolding of wild-type SNase recorded at 20 °C and pH 5.5. (A) Apparent volume change upon folding ( $\Delta V_f$ ) as a function of the protein sequence. (B) Distribution of the  $\Delta V_f$  values obtained WT SNase. (C, D) Fractional contact maps computed from the pressure-unfolding profiles of the WT-SNase at 900 and 1100 bar. The color scale is dark blue, >90% probability of contact; light blue, 80–90%; green, 70–80%; yellow, 60–70%; orange, 50–60%; and red, <50%. The circle (in D) indicates contacts that are more destabilized at these pressures than the rest of the protein.

additional cavity at the interface between the two subdomains, exhibited an asymmetric distribution of apparent  $\Delta V_f$  values at the lowest concentration (0.6 M) of GuHCl, reminiscent of that observed for the reference protein. The fractional contact maps computed for this variant from 1000 to 1400 bar at 0.6 M GuHCl (Figure 4D–F) revealed two main regions with lower probability of contact, both located in the interface between the IntD and SubD2. Disruption of contacts in these regions is consistent with the population of the major unfolding intermediate (or a very similar ensemble) observed for WT SNase and  $\Delta$ +PHS. Increasing denaturant resulted (as noted above) in an increase in the average apparent  $\Delta V_f$  for L125A and a significant narrowing of the distribution. Indeed at the highest concentration of GuHCl (0.85 M) the previously reported distribution of  $\Delta V_f$  values for this variant,<sup>8</sup> reproduced here for comparison, is much narrower and highly symmetric. Nonetheless, the standard deviation of the distribution of  $\Delta V_f$  values (~9 mL/mol), as observed for WT SNase, remains slightly larger than the average experimental uncertainty ( $\pm 6.7$  mL/mol).

In contrast to the reference protein and the L125A variant, a very broad, but symmetric, distribution of apparent  $\Delta V_f$  values was observed at the lowest GuHCl concentration (0.5 M) for the I92A variant (Figure 3E,F). This substitution located in  $\beta 5$  creates an extension of the naturally occurring cavity in the  $\beta$ -barrel in SubD1. The observed broad  $\Delta V_f$  distribution implicated regions over the entire protein structure for this variant. A global increase of the average  $\Delta V_f$  was observed with increasing GuHCl for I92A, and the distribution first broadened perceptibly, becoming more asymmetric at the intermediate

GuHCl concentration, and then narrowed slightly and became more symmetric at the highest denaturant concentration, with a large spread in standard deviation for the distribution of  $\Delta V_f$  values (~22 mL/mol), about 2-fold the average experimental uncertainty ( $\pm 13.7$  mL/mol).

The residue specific difference in the apparent  $\Delta V_f$ ,  $\Delta\Delta V_f$ , was calculated for each of the two changes in denaturant concentration for  $\Delta$ +PHS and the two cavity creating variants (Figure S3). The  $\Delta\Delta V_f$  values for  $\Delta$ +PHS were largest in the first step for residues at the interface between SubD1 and SubD2 ( $\beta 5$  and helix 2) and correspond to the denaturant-dependent suppression of the major intermediate. However, significant changes are observed throughout the protein in both steps, some of which are negative, and attest to residual underlying heterogeneity that is more apparent in SubD1 ( $\beta 1$ –3) in the second step. The  $\Delta\Delta V_f$  distributions for L125A were smaller on average and more evenly distributed than for  $\Delta$ +PHS. For I92A, the  $\Delta\Delta V_f$  values were much more heterogeneous and generally larger than for the other two variants. One residue increased by nearly 100 mL/mol in the first step, and another decreased by 40 mL/mol in the second.

**High-Pressure H/D Exchange.** The pressure dependence of H/D exchange for  $\Delta$ +PHS and for its L125A and I92A variants was investigated in the absence of chemical denaturant at 20 °C, pH 7, and pressures ranging from 1 to 2400 bar. Because of the high stability of the  $\Delta$ +PHS protein, many residues did not exchange over the observation time of the experiment at any pressure. For those that did exchange, a systematic increase in the rate of exchange (decrease in the calculated protection factors

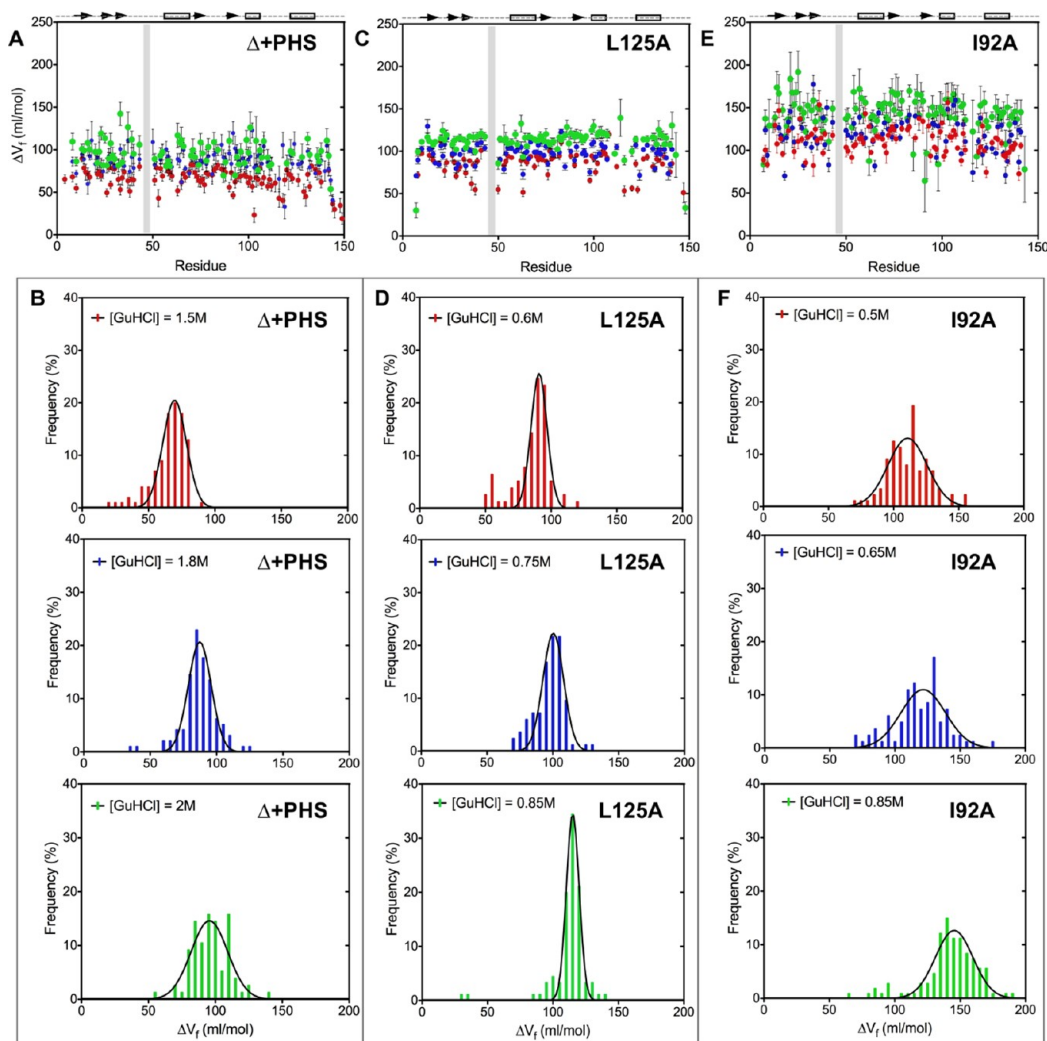


**Figure 3.** Pressure-induced unfolding of  $\Delta$ +PHS, L125A, and I92A monitored at 20 °C, pH 7, and various GuHCl concentrations. (A) Apparent volume changes for folding  $\Delta V_f$  values for  $\Delta$ +PHS as a function of the protein sequence at 1.5 M (red), 1.8 M (blue), and 2.0 M (green) GuHCl. (B) Distributions of apparent  $\Delta V_f$  values for  $\Delta$ +PHS at 1.5 M (top), 1.8 M (middle), and 2.0 M GuHCl. The data at 1.5 M GuHCl are reproduced from ref 8 for purposes of comparison. (C) Apparent volume changes for folding  $\Delta V_f$  values for L125A as a function of the protein sequence at 0.6 M (red), 0.75 M (blue), and 0.85 M (green) GuHCl. (D) Distributions of apparent  $\Delta V_f$  values for L125A at 0.6 M (top), 0.75 M (middle), and 0.85 M GuHCl. The data at 0.85 M GuHCl are reproduced from ref 8 for purposes of comparison. (E) Apparent volume changes for folding  $\Delta V_f$  values for  $\Delta$ +PHS as a function of the protein sequence at 0.5 M (red), 0.65 M (blue), and 0.85 M (green) GuHCl. (F) Distributions of apparent  $\Delta V_f$  values for I92A at 0.5 M (top), 0.65 M (middle), and 0.85 M GuHCl. The data at 0.85 M GuHCl are reproduced from ref 8 for purposes of comparison. Also for the sake of comparison, we use the same amino acid sequence length than for the WT SNase (149 residues). The gray bar indicates the location of the deletion in the  $\Delta$ +PHS background protein (residues 44–49).

(PF)) was observed with increasing pressure (Figure S4). Apparent volume changes for exchange ( $\Delta V_x$ ) were estimated from the linear dependence of the apparent free energy of exchange with pressure. Only a few residues in the IntD (residues 98, 107, 109, and 110) and in SubD2 (residue 130) exhibited  $\Delta V_x$  values above 50 mL/mol (Figure 5A). It is noteworthy that these residues are involved in a network of H-bonds around Trp 140 (Figure 5B). In contrast, H/D exchange at most of the exchangeable residues showed homogeneous  $\Delta V_x$  values around 30–40 mL/mol that were totally uncorrelated with the free energy of exchange,  $\Delta G_x$  (Figure 6). None of the  $\Delta G_x$  values reached the global folding stability of the protein ( $\Delta G_u = 11.9 \pm 0.1$  kcal/mol).

H/D exchange experiments with the L125A variant (Figure 5C) yielded very broadly distributed  $\Delta V_x$  values for several residues in

SubD1 (residues 19, 24–26, 30–34, and 37) and residues in the SubD2 (residues 129, 132, 133, and 139), well beyond the experimental uncertainty, whereas the  $\Delta V_x$  values for residues 55–110 in the center of the protein sequence were found to be highly homogeneous, near 50 mL/mol. In addition to the backbone H-bond network around Trp-140, large  $\Delta V_x$  values were also measured for several amide groups in  $\beta 1$ – $\beta 2$ – $\beta 3$  (Figure 5D). For the I92A variant (Figure 5E,F), a very broad distribution of  $\Delta V_x$  values was observed over the entire protein sequence, with the largest apparent  $\Delta V_x$  values measured in SubD1 (residues 24–25, 34, and 67–68), in the IntD (residues 104, 112, and 115), and in SubD2 (residues 131–132 and 136). In contrast to the  $\Delta$ +PHS variant, significant correlation between  $\Delta V_x$  and  $\Delta G_x$  was observed for the two cavity-containing variants (Figure 6). Strong correlations were also observed for the  $\Delta V_u$  and  $\Delta G_u$  values

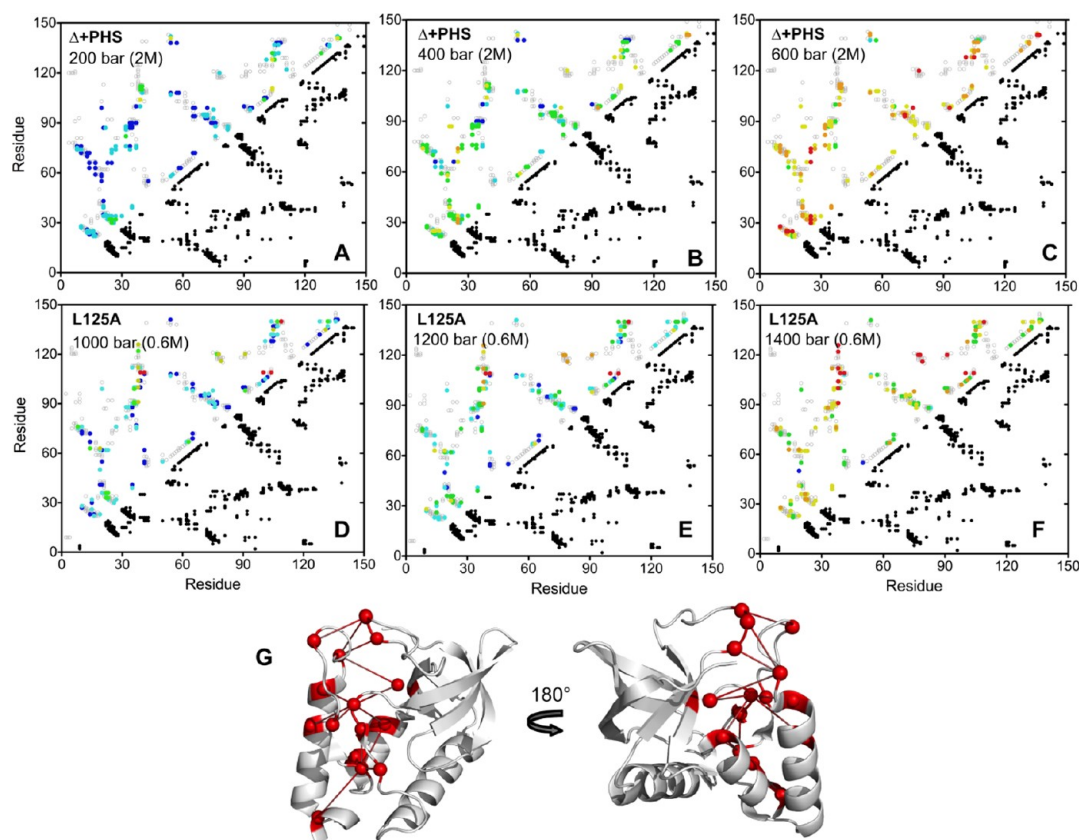


**Figure 4.** Fractional contact maps. (A–C)  $\Delta$ +PHS SNase at 2 M GuHCl and 200 (A), 400 (B), and 600 bar (C) and (D–F) L125A variant at 0.6 M GuHCl and 1000 (D), 1200 (E), and 1400 bar (F). The complete set of native contacts is represented by dark dots on the bottom half of the contact maps. The probabilities of contact, calculated as the product of the cross-peak fractional intensities of the implied pair of residues,<sup>8</sup> are indicated by color dots on the upper half of the contact maps. The color scale is dark blue, >90% probability of contact; light blue, 80–90%; green, 70–80%; yellow, 60–70%; orange, 50–60%; and red, <50%. (G) The network of native contacts of the L125A variant at 0.6 M and 1400 bar affected with a low probability of contact (<50%) are represented on the protein structure.

obtained from the high-pressure unfolding profiles for the three variants at all three denaturant concentrations.

## DISCUSSION

**Interpretation of Apparent Volume Changes for Unfolding.** The analysis of the plots of the loss of native state HSQC peak intensities as a function of pressure for nearly 100 amide groups, according to a two-state model, gives rise to distributions of apparent  $\Delta V_f (= -\Delta V_u)$  values for each of the protein variants and under each solution condition studied here and previously.<sup>8</sup> These distributions are more or less asymmetric and broad, and their average values change as well, depending upon the variant and denaturant concentration. In all cases, the standard deviation in the distribution of values was larger than the average experimental uncertainty. Strong correlation was expected and observed between  $\Delta V_u$  and  $\Delta G_u$  in the high-pressure unfolding of the variants and the reference protein at the three concentrations of denaturant. Of course, for a pure two-state unfolding transition, these curves should show a convergence of the  $\Delta V_u$  and  $\Delta G_u$  correlations for all residues toward a single value, within experimental uncertainty. The  $\Delta V_u$  and  $\Delta G_u$  values are clearly much more heterogeneous than experimental uncertainty for all variants, but this is particularly true for I92A. We interpret this heterogeneity in the values of the  $\Delta V_u$  and  $\Delta G_u$  as follows. At pressures below the unfolding midpoint, certain residues sample environments in which their amide group chemical shift is equivalent to that of the unfolded

state; hence, the intensity of the folded state peak decreases, whereas others remain in totally folded-like environments. Analysis of the individual pressure-unfolding profiles, according to a two-state model, yields very different absolute values of the apparent  $\Delta V_u$  for those residues exhibiting premature loss of peak intensity. The curves can spread over a larger pressure range, leading to a smaller absolute value for  $\Delta V_u$ , or alternately, local adjustments to pressure involving local increased solvation can lead to decreases in peak intensity over very small pressure ranges that then appear as anomalously large apparent volume changes. The degree of heterogeneity in the  $\Delta V_u$  distributions is indicative of the population of conformational excited states and unfolding intermediates, and the structural mapping of this heterogeneity allows the identification of the regions that are disrupted in these conformers. Moreover, the  $\Delta V_u$  distributions can be symmetric or asymmetric, depending upon the degree to which different intermediates are populated at different pressures and sampled by specific amide groups.

**Interpretation of Apparent Volume Changes for Exchange.** The heterogeneity in  $\Delta V_x$  values reported by H/D exchange is interpreted as a manifestation of local unfolding and hence of the probability of populating more open partially folded excited states. This has been explained in previous studies as evidence for differing pressure sensitivities of specific regions of the proteins due to local packing differences and to the population of conformers of lower volume in which these regions are opened.<sup>25</sup> In denaturant-dependent H/D exchange

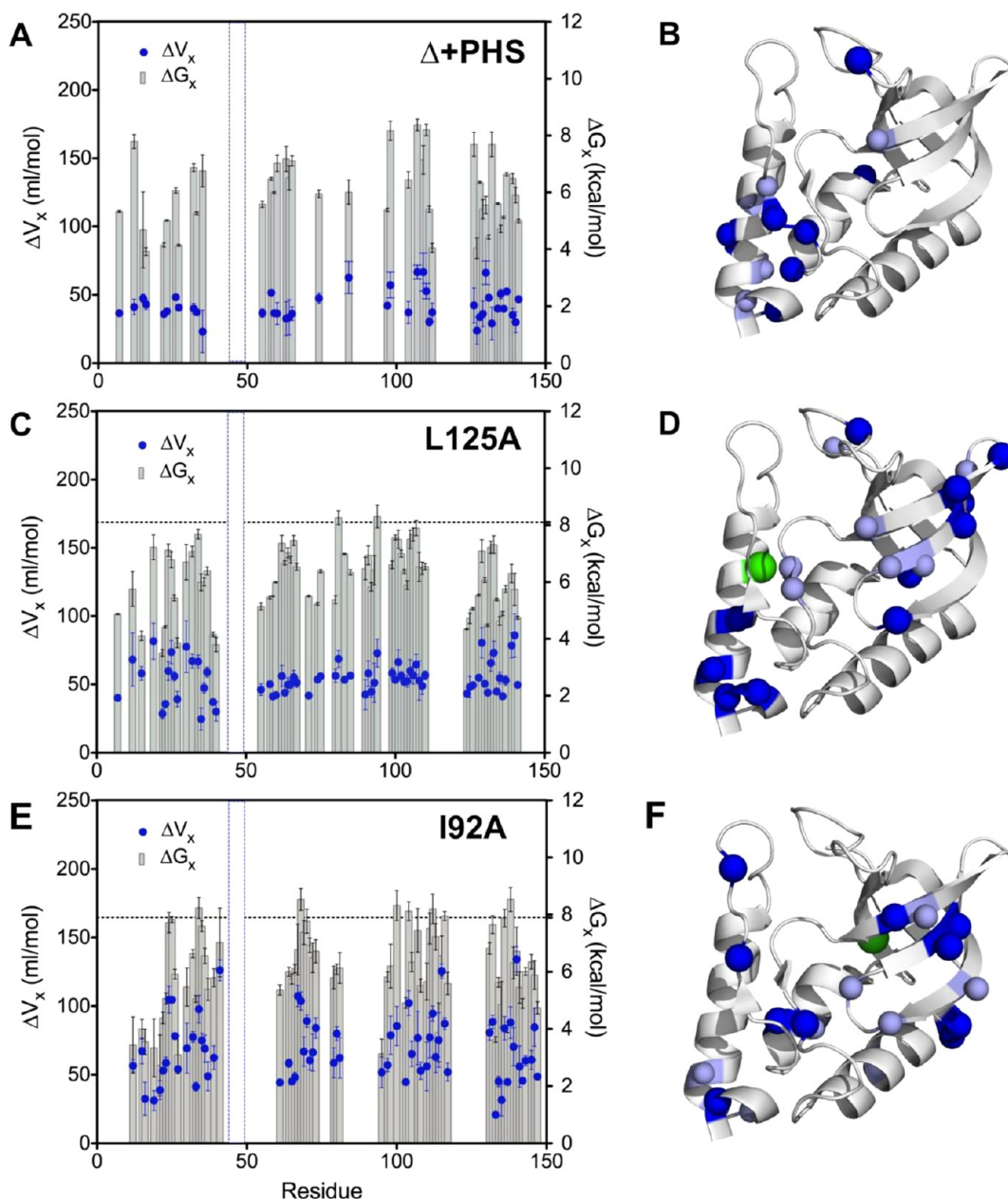


**Figure 5.** High-pressure H/D exchange results for (A)  $\Delta$ +PHS SNase, (C) L125A variant, and (E) I92A variant.  $\Delta V_x$  values are indicated with blue points and  $\Delta G_x$  values with gray bars. The dashed line indicates the global folding stability of this protein ( $8.1 \pm 0.1$  kcal/mol for L125A and  $7.9 \pm 0.3$  kcal/mol for I92A). We use the same amino acid sequence length than for the WT SNase (149 residues). The dashed blue lines indicate the location of the deletion in the  $\Delta$ +PHS background protein (residues 44–49). The outlier values of  $\Delta V_x$  are represented on the protein structure for (B)  $\Delta$ +PHS, (D) L125A variant, and (E) I92A variant centered on the  $C\alpha$  atom of each residue. The largest  $\Delta V_x$  values (more than 1 standard deviation) are indicated in dark blue, while the smallest  $\Delta V_x$  values (1 standard deviation) are colored in light blue.

of RNase A and cytochrome *c*, strong correlation was observed between the denaturant *m* values and  $\Delta G_x^{51,52}$  consistent with the idea that the exposure of more surface area involves the disruption of more interactions. A corollary relationship between  $\Delta V_x$  and  $\Delta G_x$  was observed here for the cavity-containing variants, suggesting that the amount of volume lost in partial unfolding depends upon the extent, but also surely the region and location of the structural disruption. Indeed, for the I92A variant, the cavity that exists in the central OB-fold core in the WT SNase and in  $\Delta$ +PHS has been extended by the I92A substitution. More drastic opening of the core to solvent should result in the disappearance of corresponding more solvent-excluded void volume. For L125A the correlation is significantly lower but nonetheless apparent.

For residues in the C-terminus, opening will lead to occupation of significantly more internal void volume, since the L125A substitution leads to the creation of an additional cavity between SubD2 and the IntD. H/D exchange also brought to light the population of excited states involving opening in the N-terminus, of L125A which should expose the central “WT” cavity to solvent. The larger these excursions, the more probable it is that solvent molecules enter the protein and occupy previously solvent-excluded void volume. For these proteins, higher energy locally unfolded states are energetically accessible under native conditions, leading to significant correlations between  $\Delta V_x$  and  $\Delta G_x$ . The correlation is higher for I92A than for L125A since the former accesses a larger number of excited states under native conditions.

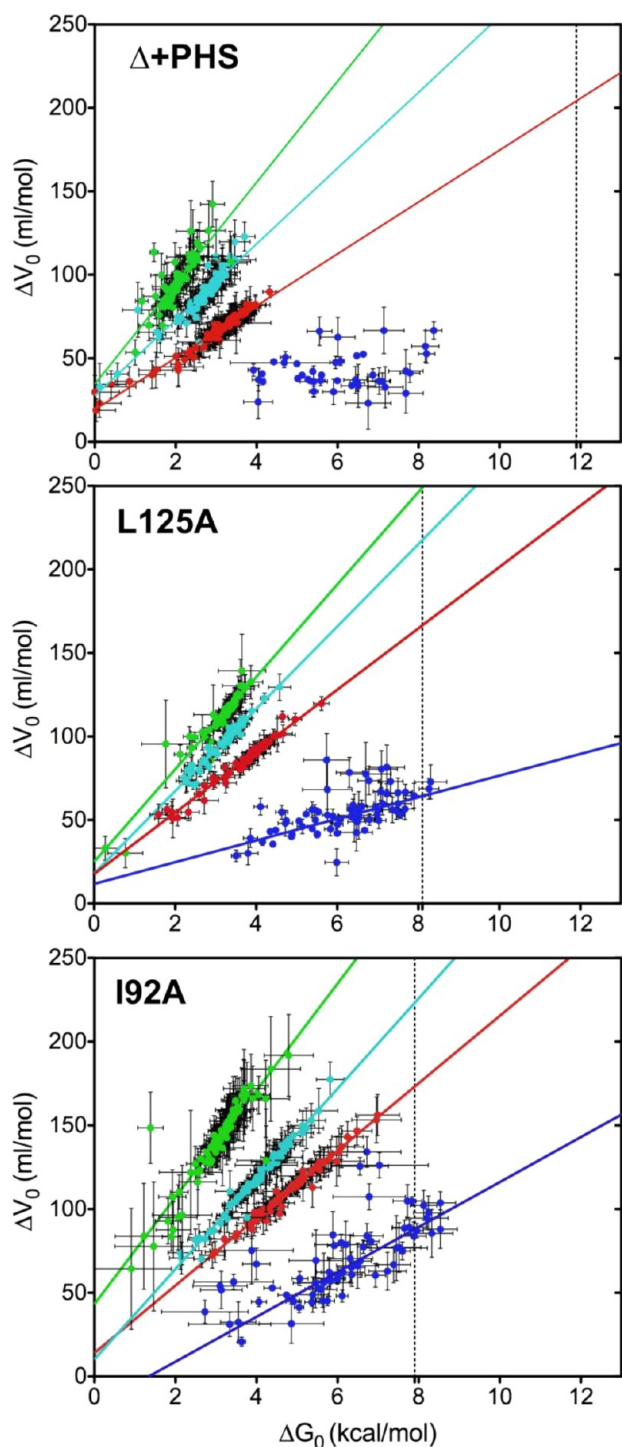


**Figure 6.** Correlations between  $\Delta V_x$  or  $\Delta V_0$  and  $\Delta G_0$  values obtained under various conditions for  $\Delta$ +PHS: 2 M GuHCl (green), 1.8 M (cyan), 1.5 M (red), H/D exchange (blue), L125A variant: 0.85 M GuHCl (green), 0.75 M (cyan), 0.6 M (red), H/D exchange (blue) and I92A variant: 0.85 M GuHCl (green), 0.65 M (cyan), 0.5 M (red), and H/D exchange (blue). The dashed line indicates the global folding stability of the protein. Data for  $\Delta$ +PHS at 1.8 M GuHCl and L125A and I92A at 0.85 M GuHCl were reproduced from ref 8.

In contrast to these strong correlations between  $\Delta V_x$  and  $\Delta G_x$  for the cavity-containing variants, there is a clear lack of a corollary relationship between  $\Delta V_x$  and  $\Delta G_x$  for the  $\Delta$ +PHS reference protein. The homogeneous and small pressure dependence of the H/D exchange observed for most of the

exchangeable residues of the reference protein may reflect the compressibility of the folded state, rather than a true volume difference between two well-defined states upon local unfolding. This response to pressure for  $\Delta$ +PHS in the absence of denaturant, conditions under which it is extremely stable, with few open conformers energetically accessible, is consistent with the notion of a general pressure-dependent increase in hydration of the folded state. This could result in a homogeneous pressure dependence of the access of the attacking hydroxide group to amide protons in all of the locally open structures, which would be more pronounced than with the model peptides used to correct the protection factors.<sup>25,51</sup> Consistent with the notion of pressure-induced increased hydration of the folded state, we previously reported a pressure dependent red-shift of the fluorescence of Trp140 at pressure where the backbone and indole amide resonances remained clearly in the folded state.<sup>8</sup>

Pressure-induced hydration of cavities has been reported for T4 lysozyme based on high-pressure crystallographic data as well as computation,<sup>53</sup> indicating that pressure (and low temperature) can act to drive water inside folded proteins.<sup>54,55</sup> However, as shown here, the conformational states with low volume that are energetically accessible to a protein under pressure depend on experimental conditions and on the individual protein. Single site mutants can exhibit very distinct behaviors. Hence, the pressure response of one protein in a crystal under cryogenic conditions is not necessarily equivalent to the response of another protein in solution or in the presence of denaturant. Nonetheless, in all these situations pressure acts to increase protein hydration and diminish the amount of solvent excluded void volume.

**Effects of Mutations on the Folding Landscape.** The most significant insight provided by the present results is how fine the line is between complexity of folding landscapes and stability in natural proteins. Increased complexity relative to the folding landscape of WT SNase was observed for both stabilizing  $\Delta$ +PHS and destabilizing alanine substitution mutations. Although the native structure of SNase encompasses two distinct structural elements, WT SNase has evolved such that the folding of these units is fairly cooperative. The equilibrium intermediate in WT SNase, which we could detect here with high pressure NMR, has only previously been detected kinetically in rapid mixing experiments.<sup>5,6</sup> The stabilizing mutations used to engineer the highly stable  $\Delta$ +PHS protein reinforce the population of this intermediate relative to the situation in the WT SNase (Figure S6).

The engineering of cavities in different subdomains of  $\Delta$ +PHS, despite having equivalent effects on global thermodynamic stability, had very different consequences on the ruggedness of the folding landscape. The consequences were relatively minor for a cavity introduced into an already frustrated region (L125A). The same intermediate, with a disrupted C-terminus, is populated as for the reference protein. While the folded state is destabilized for this variant relative to the reference protein, the intermediate is likely to be of similar free energy since the C-terminus where the mutation occurs is disordered in this intermediate (Figure S6). In addition, L125A exhibits another excited state involving the N-terminus, the relative stability of which, as judged by the  $\Delta G_x$  values, was not significantly different from the main intermediate.

In contrast, placing a cavity in a minimally frustrated region (the OB-fold core) with the I92A substitution led to significant reordering of the energetics of accessible states (Figures S5 and S6),<sup>56</sup> increasing significantly the population of multiple intermediates involving a partially unfolded central core.

The main intermediate with the disrupted C-terminus and intact OB-core domain, as for the folded state, should be significantly destabilized by the I92A substitution, since the core of the protein is folded in these two conformers. In contrast, we observed multiple intermediates exhibiting partial opening of the core. These conformers should have free energies that are higher than the WT folding barrier and thus should be inaccessible in the context of  $\Delta$ +PHS and L125A. However, they should not be significantly destabilized by the I92A mutation, and hence in this context they become accessible. We have shown that the conformations at the folding barrier for WT and  $\Delta$ +PHS resemble the main intermediate, with a collapsed and solvent excluded central core and a disrupted C-terminal helix.<sup>7</sup> This TSE must also be destabilized in I92A, and thus I92A likely folds through multiple alternate pathways involving the intermediates detected here.

The dramatic effect of the single point mutation at I92A on the roughness of the free-energy landscape illustrates the delicate balance of the native contact energetics that dictate the degree of frustration in protein folding.<sup>57,58</sup> Nevertheless, in spite of the disruption of the energetic hierarchy and the complexity of its folding pathways, the I92A variant is stably folded. Its chemical denaturation profile remains apparently as cooperative as the  $\Delta$ +PHS reference protein.<sup>36</sup> This underscores the fact that polypeptides need not have perfect funnel characteristics to be able to adopt stable structures. Indeed, selection against frustration may not always occur for proteins, depending upon their functional requirements for adaptability and dynamics.

#### Effects of Denaturant on the Folding Landscapes.

Denaturants, crowders, and osmolytes have been reported to have contradictory and strong<sup>59–61</sup> or negligible<sup>62</sup> effects on pressure-induced protein unfolding. With only tryptophan fluorescence as the observable, we previously reported no effect of GuHCl on the value of the volume change for unfolding of the SNase variants studied here.<sup>8</sup> Using over 100 observables throughout the protein sequence available with high-pressure NMR, we find that the situation is much more complex. The average apparent  $\Delta V_f$  increases with increasing denaturant for the reference  $\Delta$ +PHS protein and the two cavity variants. Beyond this general trend, the variants exhibit three distinct responses of their pressure unfolding profiles to denaturant. In the case of  $\Delta$ +PHS, denaturant suppresses the main intermediate yet increases the width of the distribution due to stabilization of alternative intermediates. Denaturant suppresses the intermediate for L125A as well but does not lead to increased heterogeneity. For I92A, multiple intermediates involving all regions of the protein are populated at all concentrations of GuHCl, which modulates their relative stability but not the overall degree of heterogeneity.

Although the detailed mechanism of action of denaturants like urea or GuHCl is controversial and still a matter of debate,<sup>63–67</sup> they are known to modify protein folding by preferentially partitioning to proteins surfaces,<sup>68</sup> differentially stabilizing extended conformational states. Such states are destabilized by molecular crowding agents and osmolytes via preferential exclusion.<sup>69</sup> The effects of cosolvents on the magnitude of  $\Delta V_f$ , where they occur, have been interpreted generally as a true change in the difference in volume between the folded and unfolded states. However, this explanation is unlikely, as we demonstrated recently that pressure unfolding of proteins is governed primarily by the existence of internal, solvent-excluded voids<sup>8</sup> and that unlike the denaturant  $m$  value,  $\Delta V_f$  is independent of the size of the protein or the polar or hydrophobic nature of the

exposed residues.<sup>70</sup> The denaturant-dependent increase in average  $\Delta V_f$  observed here is highly site specific; some residues shift significantly to higher values with increasing GuHCl, while others hardly at all, and a few even shift to lower values. Moreover,  $\Delta V_f$  does not depend upon the absolute GuHCl concentration; equivalent values are found for WT SNase and  $\Delta$ +PHS at 0 and 1.5 M GuHCl. These observations are inconsistent with an effect of denaturant on the true volume difference between folded and unfolded states. However, they can be rationalized considering the effect of denaturant on the relative stabilities of all of the possible states on the folding landscapes of the different variants and how the population of these states in an unfolding profile affects steepness of the curves and hence the apparent  $\Delta V_f$  value obtained from their fits to a two-state model. Effects of GuHCl on the complexity of folded state ensembles have been noted previously by comparing multiple observables.<sup>71</sup>

**Denaturant Effects on  $\Delta$ +PHS.** We have shown previously by p-jump kinetics and site-directed mutagenesis<sup>7</sup> that the transition state ensemble (TSE) of SNase and its  $\Delta$ +PHS variant is rather similar to the major partially folded intermediate, with a disrupted SubD2 and a concomitant loss of interfacial contacts between the two subdomains. Its higher energy relative to the intermediate can be understood in terms of a loss of tertiary interactions in a collapsed and still solvent excluded SubD1. Moreover, it is likely to represent a somewhat more solvent exposed ensemble of conformers. Hence, denaturant would be expected to have a larger stabilizing effect on the TSE, relative to the folded state, than it would for the major intermediate, the latter eventually melting into the conformations at the folding barrier and disappearing as a folding intermediate, per se, at high denaturant concentrations. At the same time, other higher energy partially folded states involving SubD1, which are sparsely populated in absence of GuHCl, would also be stabilized by denaturant since they involve solvent exposure. This would increase the conformational heterogeneity on the folded side of the barrier and would result in a broad and much more symmetric  $\Delta V_f$  distribution. Since folding proceeds via a TSE bearing a largely compact SubD1, these additional partially folded states are off-pathway (with corresponding TSE's that are much higher in energy).

**Denaturant Effects on L125A.** The situation concerning the suppression of the intermediate is quite similar for the L125A variant. In contrast, while the free energy difference between the folded state and the intermediate, and the free energy difference between the folded state and the TSE, are much smaller for L125A, since the mutation perturbs interactions at the interface between SubD1 and SubD2, this is not the case for the other partially folded states on the folding landscape, which involve disruption of interactions in SubD1. Hence, the suppression of the main intermediate by GuHCl results in a much more symmetric distribution of  $\Delta V_f$  values, as noted above for  $\Delta$ +PHS, but the relative stability changes brought on by the mutation preclude the GuHCl-dependent population of other intermediates and give rise, at the highest concentration of GuHCl, to a significantly narrower distribution of  $\Delta V_f$  values compared to  $\Delta$ +PHS.

**Denaturant Effects on I92A.** Because of the fact that the destabilizing mutation of I92A is located in the most deeply buried, stable region of the protein (SubD1, foldon 2), the free energy difference between the folded state and multiple excited states on the folded side of the barrier is diminished, and these latter are much more readily populated. It is also likely that this

mutation results in multiple unfolding pathways. Denaturant reshuffles all of the states on this complex landscape, stabilizing some with respect to others, such that  $\Delta V_f$  values increase dramatically with denaturants for some residues, whereas for others there is little change or even a decrease.

## CONCLUSION

The consequences of stabilizing or cavity-creating mutations and chemical denaturant on the folding free energy landscape of SNase were characterized in exquisite detail by combining pressure perturbation with the site-specific information afforded by NMR spectroscopy. Significant deviation from simple two-state unfolding was revealed via the determination of apparent volume differences between folded, partially folded, and unfolded states at over 100 residues in each protein variant and under many conditions. Excited-state populations were also probed by pressure-dependent NMR H/D exchange measurements. Mutations strongly affected the ruggedness of the folding free energy landscape. That of the true wild-type form of SNase was nearly entirely smooth, while the major intermediate, involving a disrupted C-terminus, was significantly enhanced by the stabilizing mutations of  $\Delta$ +PHS. We observed very distinct effects of the two alanine substitutions on the free energy landscape, despite their equivalent effects on global stability. Specifically, the L125A substitution led to the population of excited states involving disruption of the N-terminus as well as the major folding intermediate. However, because of the local energetic consequences of the mutation, the folding landscape of this variant became nearly perfectly smooth upon increasing denaturant. In contrast, the I92A substitution significantly increased the roughness of the folding free energy landscape, leading to multiple partially folded states involving the core of the protein. The detailed insights about folding pathways obtained from these pressure perturbation experiments stem from the fact that pressure is a fairly mild perturbation since its effects originate from the heterogeneously distributed packing properties of the folded protein and not from a general effect of exposed surface area. Coupling pressure perturbation with site-specific NMR measurements has provided unprecedented descriptions of these folding free energy landscapes, with implications for adaptive evolution, folding-based diseases, and protein design.

## ASSOCIATED CONTENT

### Supporting Information

Figure S1: examples of pressure unfolding profiles recorded at 20 °C for the wt SNase; Figure S2: comparison of the free energy profiles obtained from Go model simulations of  $\Delta$ +PHS at different concentrations of GuHCl; Figure S3: change in the apparent  $\Delta V_f$  as a function of the GuHCl concentration; Figure S4: H/D exchange experiments performed on  $\Delta$ +PHS at 20 °C, pD = 7, and pressures ranging from 1 to 2400 bar; Figure S5: localization of the frustrated and minimally frustrated network of contacts in the  $\Delta$ +PHS structure (3BDC); Figure S6: schematic free energy diagrams for the nuclease variants studied. This material is available free of charge via the Internet at <http://pubs.acs.org>.

## AUTHOR INFORMATION

### Corresponding Author

\*E-mail [catherine.royer@cbs.cnrs.fr](mailto:catherine.royer@cbs.cnrs.fr); Tel +33 467 41 79 02.

## Notes

The authors declare no competing financial interest.

## ACKNOWLEDGMENTS

We gratefully acknowledge support from the Agence National de la Recherche grant PiriBio 09-455024 (C.A.R.), grants MCB-0743422 (B.G.M.E.) and MCB-0543769 and MCB-1050966 (A.E.G.) from the National Science Foundation. D.R.N. was supported by a fellowship from Coordination for the Training and Improvement of Higher Education Personnel (CAPES) of Brazil, and J.R. was supported by a fellowship from the French Ministry of Research and Higher Education and a Fulbright International Graduate Fellowship.

## ABBREVIATIONS

$\Delta$ +PHS, hyperstable form of staphylococcal nuclease; GuHCl, guanidinium hydrochloride; H/D, hydrogen/deuterium; HSQC, heteronuclear single quantum coherence; IntD, interdomain; NMR, nuclear magnetic resonance; OB, oligonucleotide/oligosaccharide-binding; SNase, staphylococcal nuclease; SubD1, subdomain 1; SubD2, subdomain 2; TSE, transition-state ensemble.

## REFERENCES

- (1) Taniuchi, H., and Anfinsen, C. B. (1969) An experimental approach to the study of the folding of the Staphylococcal nuclease. *J. Biol. Chem.* 244, 3864–3875.
- (2) Shortle, D., Meeker, A. K., and Freire, E. (1988) Stability mutants of staphylococcal nuclease: large compensating enthalpy-entropy changes for the reversible denaturation reaction. *Biochemistry* 27, 4761–4768.
- (3) Murzin, A. G. (1993) OB(oligonucleotide/oligosaccharide binding)-fold: common structural and functional solution of non-homologous sequences. *EMBO J.* 12, 861–867.
- (4) Bedard, S., Mayne, L. C., Petersen, R. W., Wand, A. J., and Englander, S. W. (2008) The foldon substructure of staphylococcal nuclease. *J. Mol. Biol.* 376, 1142–1154.
- (5) Maki, K., Cheng, H., Dolgikh, D. A., Shastry, M. C., and Roder, H. (2004) Early events during folding of wild-type staphylococcal nuclease and a single-tryptophan variant studied by ultrarapid mixing. *J. Mol. Biol.* 338, 383–400.
- (6) Maki, K., Cheng, H., Dolgikh, D. A., and Roder, H. (2007) Folding kinetics of staphylococcal nuclease studied by tryptophan engineering and rapid mixing methods. *J. Mol. Biol.* 368, 244–255.
- (7) Mitra, L., Hata, K., Kono, R., Isom, D., Rouget, J.-B., Winter, R., Akasaka, K., Garcia-Moreno, B., and Royer, C. A. (2007) V-value analysis: a pressure-based method for mapping the folding transition state ensemble of proteins. *J. Am. Chem. Soc.* 129, 14108–14109.
- (8) Roche, J., Caro, J. A., Norberto, D. R., Barthe, P., Roumestand, C., Schlessman, J. L., Garcia, A. E., Garcia-Moreno, B., and Royer, C. A. (2012) Cavities determine the pressure unfolding of proteins. *Proc. Natl. Acad. Sci. U. S. A.* 109, 6945–6950.
- (9) Cellitti, J., Llinas, M., Echols, N., Shank, E. A., Gillespie, B., Kwon, E., Crowder, S. M., Dahlquist, F. W., Alber, T., and Marqusee, S. (2007) Exploring subdomain cooperativity in T4 lysozyme I: structural and energetic studies of a circular permutant and protein fragment. *Protein Sci.* 16, 842–851.
- (10) Cellitti, J., Bernstein, R., and Marqusee, S. (2007) Exploring subdomain cooperativity in T4 lysozyme II: uncovering the C-terminal subdomain as a hidden intermediate in the kinetic folding pathway. *Protein Sci.* 16, 852–861.
- (11) Kiefhaber, T., Labhardt, A. M., and Baldwin, R. L. (1995) Direct NMR evidence for an intermediate preceding the rate-limiting step in the unfolding of ribonuclease A. *Nature* 375, 513–515.
- (12) Houry, W. A., and Scheraga, H. A. (1996) Structure of a hydrophobically collapsed intermediate on the conformational folding

pathway of ribonuclease A probed by hydrogen-deuterium exchange. *Biochemistry* 35, 11734–11746.

(13) Matagne, A., Chung, E. W., Ball, L. J., Radford, S. E., Robinson, C. V., and Dobson, C. M. (1998) The origin of the alpha-domain intermediate in the folding of hen-lysozyme. *J. Mol. Biol.* 277, 997–1005.

(14) Hoang, L., Bedard, S., Krishna, M. M., Lin, Y., and Englander, S. W. (2002) Cytochrome c folding pathway: kinetic native-state hydrogen exchange. *Proc. Natl. Acad. Sci. U. S. A.* 99, 12173–12178.

(15) Baldwin, R. L., Frieden, C., and Rose, G. D. (2010) Dry molten globule intermediates and the mechanism of protein folding. *Proteins* 78, 2725–2737.

(16) Dobson, C. M. (2003) Protein folding and misfolding. *Nature* 426, 884–890.

(17) Luheshi, L. M., and Dobson, C. M. (2009) Bridging the gap: from protein misfolding to protein misfolding diseases. *FEBS Lett.* 583, 2581–2586.

(18) Naem, A., and Fazili, N. A. (2011) Defective protein folding and aggregation as the basis of neurodegenerative diseases: the darker aspect of proteins. *Cell Biochem. Biophys.* 61, 237–250.

(19) Neudecker, P., Lundstrom, P., and Kay, L. E. (2009) Relaxation dispersion NMR spectroscopy as a tool for detailed studies of protein folding. *Biophys. J.* 96, 2045–2054.

(20) Korzhnev, D. M., and Kay, L. E. (2008) Probing invisible, low-populated states of protein molecules by relaxation dispersion NMR spectroscopy: an application to protein folding. *Acc. Chem. Res.* 41, 442–451.

(21) Neudecker, P., Robustelli, P., Cavalli, A., Walsh, P., Lundstrom, P., Zarrine-Afsar, A., Sharpe, S., Vendruscolo, M., and Kay, L. E. (2012) Structure of an intermediate state in protein folding and aggregation. *Science* 336, 362–366.

(22) Bai, Y., Sosnick, T. R., Mayne, L., and Englander, S. W. (1995) Protein folding intermediates: native-state hydrogen exchange. *Science* 269, 192–197.

(23) Krishna, M. M. G., Hoang, L., Lin, Y., and Englander, S. W. (2004) Hydrogen exchange methods to study protein folding. *Methods* 34, 51–64.

(24) Maity, H., Lim, W. K., Rumbley, J. N., and Englander, S. W. (2003) Protein hydrogen exchange mechanism: local fluctuations. *Protein Sci.* 12, 153–160.

(25) Fuentes, E. J., and Wand, J. A. (1998) Local stability and dynamics of apocytochrome b<sub>562</sub> examined by the dependence of hydrogen exchange on hydrostatic pressure. *Biochemistry* 37, 9877–9883.

(26) Akasaka, K., and Li, H. (2001) Low-lying excited states of proteins revealed from non-linear pressure shifts in <sup>1</sup>H and <sup>15</sup>N NMR. *Biochemistry* 40, 8665–8671.

(27) Kitahara, R., Yamada, H., and Akasaka, K. (2001) Two folded conformers of ubiquitin revealed by high-pressure NMR. *Biochemistry* 40, 13556–13563.

(28) Kitahara, K., and Akasaka, K. (2003) Close identity of a pressure-stabilized intermediate with a kinetic intermediate in protein folding. *Proc. Natl. Acad. Sci. U. S. A.* 100, 3167–3172.

(29) Inoue, K., Yamada, H., Akasaka, K., Hermann, C., Kremer, W., Maurer, T., Doker, R., and Kalbitzer, H. R. (2000) Pressure-induced local unfolding of the Ras binding domain of RalGDS. *Nat. Struct. Biol.* 7, 547–550.

(30) Kitahara, R., Yamada, H., Akasaka, K., and Wright, P. E. (2002) High-pressure NMR reveals that apomyoglobin is an equilibrium mixture from the native to the unfolded. *J. Mol. Biol.* 320, 311–319.

(31) Akasaka, K. (2006) Probing conformational fluctuations of proteins by pressure perturbation. *Chem. Rev.* 106, 1814–1835.

(32) Eriksson, A. E., Baase, W. A., Zhang, X. J., Heinz, D. W., Blaber, M., Baldwin, E. P., and Matthews, B. W. (1992) Response of a protein structure to cavity-creating mutations and its relation to the hydrophobic effect. *Science* 255, 178–183.

(33) Shortle, D., Stites, W. E., and Meeker, A. K. (1990) Contributions of the large hydrophobic amino acids to the stability of Staphylococcal Nuclease. *Biochemistry* 29, 8033–8041.

(34) Loladze, V. V., Ermolenko, D. N., and Makhatadze, G. I. (2002) Thermodynamic consequences of burial of polar and non-polar amino acid residues in the protein interior. *J. Mol. Biol.* 320, 343–357.

(35) Fersht, A. R., and Sato, S. (2004)  $\phi$ -value analysis and the nature of protein-folding transition states. *Proc. Natl. Acad. Sci. U. S. A.* 101, 7976–7981.

(36) Roche, J., Caro, J. A., Dellarole, M., Guca, E., Royer, C. A., Garcia-Moreno, B., Garcia, A. E., and Roumestand, C. Structural, energetic and dynamic responses of the native state ensemble to cavity-creating mutations, submitted for publication.

(37) Shortle, D., and Meeker, A. K. (1989) Residual structure in large fragments of staphylococcal nuclease: effects of amino acid substitutions. *Biochemistry* 28, 936–944.

(38) Castañeda, C. A., Fitch, C. A., Majumbar, A., Khangulov, V., Schlessman, J. L., and Garcia-Moreno, E. B. (2009) Molecular determinants of the pK<sub>a</sub> values of Asp and Glu residue in staphylococcal nuclease. *Proteins* 77, 570–588.

(39) Piotto, M., Saudek, V., and Sklenar, V. (1992) Gradient-tailored excitation for single-quantum NMR spectroscopy of aqueous solutions. *J. Biomol. NMR* 2, 661–665.

(40) Sklenar, V. (1990) Selective excitation techniques for water suppression in one- and two-dimensional NMR spectroscopy. *Basic Life Sci.* 56, 63–84.

(41) Pons, J. L., Malliavin, T. E., and Delsuc, M. A. (1996) Gifa V. 4: A complete package for NMR data set processing. *J. Biomol. NMR* 8, 445–452.

(42) Bodenhausen, G., and Ruben, D. J. (1980) Natural abundance nitrogen-15 NMR by enhanced heteronuclear spectroscopy. *Chem. Phys. Lett.* 69, 185–189.

(43) Kitahara, R., Hata, K., Maeno, A., Akasaka, K., Chimenti, M. S., Garcia-Moreno, B. E., Schroer, M. A., Jeworrek, C., Tolan, M., Winter, R., Roche, J., Roumestand, C., Montet de Guillen, K., and Royer, C. A. (2011) Structural plasticity of staphylococcal nuclease probed by perturbation with pressure and pH. *Proteins* 79, 1293–1305.

(44) Bai, Y., Milne, J. S., Mayne, L., and Englander, S. W. (1993) Primary structure effects on peptide group hydrogen exchange. *Proteins* 17, 75–86.

(45) Noel, J. K., Whitford, P. C., Sanbonmatsu, K. Y., and Onuchic, J. N. (2010) SMOG@ctbp: simplified deployment of structure-based models in GROMACS. *Nucleic Acids Res.* 38 (Web server issue), W657–W661.

(46) Ferrenberg, A. M., and Swendsen, R. H. (1988) New Monte Carlo technique for studying phase transitions. *Phys. Rev. Lett.* 61, 2635–2638.

(47) Ferrenberg, A. M., and Swendsen, R. H. (1989) Optimized Monte Carlo data analysis. *Phys. Rev. Lett.* 63, 1195–1198.

(48) Wang, M., Feng, Y., Yao, H., and Wang, J. (2010) Importance of the C-terminal loop L137-S141 for the folding and folding stability of staphylococcal nuclease. *Biochemistry* 49, 4318–4326.

(49) Whitten, S. T., and Garcia-Moreno, E. B. (2000) pH dependence of stability of staphylococcal nuclease: evidence of substantial electrostatic interactions in the denaturated state. *Biochemistry* 39, 14292–14304.

(50) Brun, L., Isom, D. G., Velu, P., Garcia-Moreno, B., and Royer, C. A. (2006) Hydration of the folding Transition State Ensemble of a protein. *Biochemistry* 45, 3473–3480.

(51) Mayo, S. L., and Baldwin, R. L. (1993) Guanidinium chloride induction of partial unfolding in amide proton exchange in RNase A. *Science* 262, 873–876.

(52) Bai, Y., Sosnick, T. R., Mayne, L., and Englander, S. W. (1995) Protein folding intermediates: native-state hydrogen exchange. *Science* 269, 192–197.

(53) Collins, M. D., Hummer, G., Quillin, M. L., Matthews, B. W., and Gruner, S. M. (2005) Cooperative water filling of a nonpolar protein cavity observed by high-pressure crystallography and simulation. *Proc. Natl. Acad. Sci. U. S. A.* 102, 16668–16671.

(54) Halle, B. (2004) Biomolecular cryocrystallography: structural changes during flash-cooling. *Proc. Natl. Acad. Sci. U. S. A.* 101, 4793–4798.

- (55) Hummer, G., Garde, S., Garcia, A. E., Paulaitis, M. E., and Pratt, L. R. (1998) The pressure dependence of hydrophobic interactions is consistent with the observed pressure denaturation of proteins. *Proc. Natl. Acad. Sci. U. S. A.* 95, 1552–1555.
- (56) Jenik, M., Parra, R. G., Radusky, L. G., Turjanski, A., Wolynes, P. G., and Ferreiro, D. U. (2012) Protein frustratometer: a tool to localize energetic frustration in protein molecules. *Nucleic Acids Res.* 40 (Web server issue), W348–W351.
- (57) Ferreiro, D. U., Hegler, J. A., Komives, E. A., and Wolynes, P. G. (2007) Localizing frustration in native proteins and protein assemblies. *Proc. Natl. Acad. Sci. U. S. A.* 104, 19819–19824.
- (58) Ferreiro, D. U., Hegler, J. A., Komives, E. A., and Wolynes, P. G. (2008) On the role of frustration in the energy landscapes of allosteric proteins. *Proc. Natl. Acad. Sci. U. S. A.* 108, 3499–3503.
- (59) Suarez, M. C., Rocha, C. B., Sorenson, M. M., Silva, J. L., and Foguel, D. (2008) Free-energy linkage between folding and calcium binding in EF-hand proteins. *Biophys. J.* 95, 4820–4828.
- (60) Wang, S., Tate, M., and Gruner, S. M. (2012) Protein crowding impedes pressure-induced unfolding of Staphylococcal nuclease. *Biochim. Biophys. Acta* 1820, 957–961.
- (61) Oliveira, A. C., Gaspar, L. P., Da Poain, A. T., and Silva, J. L. (1994) Arc repressor will not denature under pressure in the absence of water. *J. Mol. Biol.* 240, 184–187.
- (62) Frye, J. K., Perman, C. S., and Royer, C. A. (1996) Testing the correlation between  $\Delta A$  and  $\Delta V$  of protein unfolding using m value mutants of staphylococcal nuclease. *Biochemistry* 35, 10234–10239.
- (63) Schellman, J. A. (2002) Fifty years of solvent denaturation. *Biophys. Chem.* 96, 91–101.
- (64) Auton, M., Holthauzn, L. M. F., and Bolen, W. D. (2007) Anatomy of energetic changes accompanying urea-induced protein denaturation. *Proc. Natl. Acad. Sci. U. S. A.* 104, 15317–15322.
- (65) Canchi, D. R., and Garcia, A. E. (2011) Backbone and side-chain contributions in protein denaturation by urea. *Biophys. J.* 100, 1526–1533.
- (66) Canchi, D. R., Pascheck, D., and Garcia, A. E. (2010) Equilibrium study of protein denaturation by urea. *J. Am. Chem. Soc.* 132, 2338–2344.
- (67) Guinn, E. J., Pegram, L. M., Capp, M. W., Pollock, M. N., and Record, T. M., Jr. (2011) Quantifying why urea is a protein denaturant, whereas glycine betaine is a stabilizer. *Proc. Natl. Acad. Sci. U. S. A.* 108, 16932–16937.
- (68) Myers, J. K., Pace, C. N., and Scholtz, J. M. (1995) Denaturant m values and heat capacity changes: relation to changes in accessible surface areas of protein unfolding. *Protein Sci.* 4, 2138–2148.
- (69) Hong, J., and Gierasch, L. M. (2010) Macromolecular crowding remodels the energy landscape of a protein by favoring a more compact unfolded state. *J. Am. Chem. Soc.* 132, 10445–10452.
- (70) Rouget, J. B., Aksel, T., Roche, J., Saldana, J. L., Garcia, A. E., Barrick, D., and Royer, C. A. (2011) Size and sequence and the volume change of protein folding. *J. Am. Chem. Soc.* 133, 6020–6027.
- (71) Ferreon, A. C., and Bolen, D. W. (2004) Thermodynamics of denaturant-induced unfolding of a protein that exhibits variable two-state denaturation. *Biochemistry* 43, 13357–13369.